Agricultural Water Management 325 (2026) 110191

Contents lists available at ScienceDirect

Agricultural Water Management

journal homepage: www.elsevier.com/locate/agwat

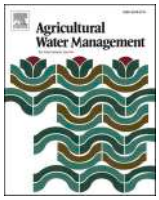

Impact of the soil freeze-thaw process on runoff generation and water balance in an alpine region of the northeast Qinghai-Tibet plateau

Linshan Yang [a,b,*], Jingru Wang [a,b,c], Tiaoxue Lu [a,b,c], Wanghan He [a,b,c], Xingyi Zou [a,b,c], Honghua Xia [a,b,c], Raffaele Albano [d], Bogdan Ozga-Zielinski [e], Jan Adamowski [f], Qi Feng [a,b]

[a] State Key Laboratory of Ecological Safety and Sustainable Development in Arid Lands, Northwest Institute of Eco-Environment and Resources, Chinese Academy of Sciences, Lanzhou 730000, China
[b] Qilian Mountains Eco-Environment Research Center in Gansu Province, Lanzhou 730000, China
[c] University of Chinese Academy of Sciences, Beijing 100049, China
[d] School of Engineering, University of Basilicata, Potenza 85100, Italy
[e] Centre of Hydrology, National Research Institute, Institute of Meteorology and Water Management, Warsaw PL-01-673, Poland
[f] Department of Bioresource Engineering, Faculty of Agricultural & Environmental Sciences, McGill University, Quebec H9X 3V9, Canada

ARTICLE INFO

Handling Editor - Dr. Brent Clothier

Keywords:
Freeze-thaw process
Runoff generation
Water balance
SHAW
Qilian Mountains

ABSTRACT

The soil freeze-thaw process profoundly influences runoff generation through complex and interconnected mechanisms, yet its quantitative impact remains poorly understood, particularly across different vegetation types and elevations. Addressing this issue is critical for improving hydrological predictions in cold regions. In this study, we established an integrated atmosphere-vegetation-soil observation system across varying elevations and vegetation types in the Qilian Mountains (QLM) and employed the Simultaneous Heat and Water (SHAW) model to quantitatively assess soil hydrothermal dynamics and runoff generation during different freeze-thaw stages from 2015 to 2023. The results demonstrate that the SHAW model could accurately simulate soil hydrothermal processes across all vegetation types (NSE > 0.80 for soil temperature; NSE > 0.69 for soil moisture) in an alpine region. Soil water content and water balance components varied significantly across both freeze-thaw stages and vegetation types. There was almost no surface runoff formed in desert steppe and mountainous steppe, and deep seepage was also low. In contrast, shrub meadow exhibited substantial deep seepage (89.29 mm) during the completely thawed stage and could be a major source of recharging to streamflow. The major water fluxes for the four vegetation types occurred during thawing and completely thawed stages, dominated by evapotranspiration. Evapotranspiration accounted for 93 %, 94 %, 81 %, and 62 % of annual precipitation in desert steppe, mountainous steppe, coniferous forest, and shrub meadow, respectively. While the component of evapotranspiration differed, it was dominated by soil evaporation in desert steppe (79 % of total ET) and mountainous steppe (92 %), and by vegetation transpiration in coniferous forest (59 %) and shrub meadow (78 %). These findings offer critical insights into water partitioning within the soil-vegetation-atmosphere continuum, enabling more accurate predictions of streamflow and water availability in alpine regions.

1. Introduction

Alpine regions are characterized by unique ecological and hydrological complexities (Gao et al., 2020; Walvoord and Kurylyk, 2016; Zhao et al., 2024), driven by pronounced variations in temperature, precipitation, and vegetation (Connon et al., 2014; Dobiński, 2020; Wu et al., 2023; Yang et al., 2020). As the largest high-altitude permafrost region in the mid-latitudes, the Qinghai–Tibet Plateau (QTP) exhibits extensive distribution of permafrost and seasonally frozen ground, which profoundly influences regional hydrology, ecosystem stability, and carbon cycling (Dobiński, 2020; Lamontagne-Hallé et al., 2018). The soil freeze-thaw process, a natural phenomenon driven by seasonal temperature variations, plays a critical role in shaping the hydrological cycle of alpine regions (Gao et al., 2023). It involves the cyclic freezing

* Corresponding author at: State Key Laboratory of Ecological Safety and Sustainable Development in Arid Lands, Northwest Institute of Eco-Environment and Resources, Chinese Academy of Sciences, Lanzhou 730000, China.
E-mail address: yanglsh08@lzb.ac.cn (L. Yang).

https://doi.org/10.1016/j.agwat.2026.110191
Received 13 July 2025; Received in revised form 22 January 2026; Accepted 22 January 2026
Available online 27 January 2026

and thawing of soil water (Zhao et al., 2022), and stands out as a pivotal factor with far-reaching consequences (Wang et al., 2023b). This process is especially pronounced in alpine regions like the QTP, where extreme cold during winter leads to the soil becoming completely frozen, followed by thawing during spring and summer (Ming et al., 2022). Investigating the freeze-thaw process impact on hydrological processes in alpine regions is essential for understanding soil-water-climate interactions, offering insights into water partitioning and storage within the soil-vegetation-atmosphere continuum, enabling more accurate predictions of streamflow patterns and water availability.

The freeze-thaw process modifies soil physical properties by altering structure and porosity (Hu et al., 2023; Wang et al., 2020), therefore, it can significantly influence runoff generation mechanisms as well as basin-scale water balance (Connon et al., 2014; Walvoord and Kurylyk, 2016). As water within the soil pores freezes, it expands, causing the soil particles to move apart, thus increasing soil porosity (Dobiński, 2020). Such expansion often generates cracks and fissures (Rooney et al., 2022), creating preferential flow paths that modify water infiltration and runoff patterns. During thawing stages, subsequent ice melt and water release further modify soil structure (Dong et al., 2023). These structural modifications can have a direct impact on the soil's ability to store and release water, thereby influencing the water yield regime.

The freeze-thaw process critically influences basin hydrology by altering soil infiltration capacity (Gao et al., 2020), thereby affecting water partitioning among soil moisture, evaporation, transpiration, and runoff (Gao et al., 2022; You et al., 2017). As the soil freezes, ice formation in soil pores reduces permeability, thereby decreasing infiltration (Peng et al., 2017). This reduction enhances surface runoff and curtails groundwater recharge, as precipitation is impeded by the frozen soil (Cheng et al., 2024). Additionally, solid soil water becomes unavailable for evaporation or transpiration, reducing these fluxes. Conversely, during thawing, the melting of solid water restores soil permeability and infiltration (Wu et al., 2023), enhancing groundwater recharge while decreasing surface runoff (Wang et al., 2019b; Wang and Gao, 2022). The subsequent release of liquid water also increases its availability for evaporation and transpiration (Gao et al., 2023).

However, due to the difficulty of frozen soils' hydraulic and thermal properties being directly measured in situs (Hu et al., 2015) and considerable uncertainty in laboratory analyses as well (Chen et al., 2015), studying the effects of soil freeze-thaw processes on runoff generation in alpine regions presents significant challenges. Furthermore, hydrological models that incorporate freeze-thaw processes typically require numerous spatially distributed parameters, which are often inaccurate or unavailable due to environmental heterogeneity and harsh conditions (Chen et al., 2018). While common practice involves parameter calibration with observed targets (e.g., streamflow, evaporation), the freeze-thaw process itself is rarely validated, introducing substantial uncertainties. Therefore, one-dimensional models that couple the physical processes of water and heat transfer, combined with accurate observations of the atmosphere-vegetation-soil system, have become the preferred choice for simulating the soil freeze-thaw process. These models provide valuable insights into alpine runoff generation mechanisms that cannot be directly observed (Zhao et al., 2024). Among these, the Simultaneous Heat and Water (SHAW) model (Flerchinger and Saxton, 1989), coupled heat and mass transfer model (CoupModel) (Jansson, 2012) and Hydrus–1D model (Hansson et al., 2004) incorporate soil water and heat interactions and have been widely used to investigate runoff generation and water balance in frozen regions (Wang et al., 2023b; Zheng et al., 2023). The SHAW model, selected for use in this study, effectively simulates coupled water and heat processes in frozen soil by accounting for soil water movement, heat conduction, and vegetation dynamics (Hu et al., 2023; Langford et al., 2020). Extensive research has validated the SHAW model's efficiency in simulating hydrothermal characteristics in frozen environments (Wang et al., 2023a; Cheng et al., 2024), including heat, water, and solute transport, as well as the impacts of vegetation and snow cover (Langford et al., 2020). Additionally, it has been applied to simulate the soil freeze-thaw process at different groundwater depths (Cheng et al., 2024). The results demonstrated that the SHAW model can not only accurately capture the temporal variations of soil temperature and liquid water in the freeze-thaw process, but also effectively simulate the solid water, reflecting the mutual transformation of liquid and solid water in the soil freeze-thaw process (Lu et al., 2025).

The Qilian Mountains (QLM), situated on the northeastern margin of the Qinghai-Tibet Plateau, feature high elevations and extremely low temperature. Approximately 96 % of the area contains permafrost and seasonally frozen ground (Zou et al., 2017). As a critical water source for mid-downstream oases, QLM streamflow sustains ecosystems throughout the Hexi Corridor (Yang et al., 2024). However, the hydrological contributions from extensive shallow mountain areas remain uncertain due to a lack of observational data, which hinders comprehensive water resource management. Although freeze-thaw cycles in these regions are likely to significantly influence water yield and balance, their specific impacts on runoff generation mechanisms are still not well understood and require further investigation.

Therefore, based on an integrated atmosphere-vegetation-soil observation system established across different elevations and vegetation types in the Qilian Mountains (QLM), this study aims to investigate the spatial heterogeneity of soil freeze-thaw process under different vegetation types, characterize runoff regimes during various freeze-thaw stages, and examine the relationship between freeze-thaw process and runoff formation in alpine regions. The aims of this study are: (1) to analyze the soil freeze-thaw process among different vegetation types (desert steppe, coniferous forest, mountainous steppe and shrub meadow); (2) to investigate the heterogeneity of runoff formation process and water balance in different freeze-thaw stages; and (3) to clarify the mechanism influencing the soil freeze-thaw process on runoff generation and water balance. The findings could be utilized to enable more accurate predictions of streamflow and water availability, thereby informing integrated water resources management in alpine regions.

2. Materials and methods

2.1. Study area

The study area, Dakouzi watershed (DKW), is located in the northeast region of the Qinghai-Tibet plateau (Fig. 1). This small, narrow watershed extends from southwest to northeast laying between 38°36′N to 38°39′N and 100°15′E to 100°19′E. It covers an area of 6.59 km^2 with a length of 7.2 km and a maximum width of 1.4 km. Elevations range from 2109 m to 3558 m, with slopes varying between 6° and 60° (Fig. 1). The landscapes include desert steppe, mountainous steppe, coniferous forest and shrub meadow within the elevation varying from low to high. Soil types are mainly chestnut soil at low elevation and gray cinnamon soil at high elevation. In contrast to the other existing small watershed observation sites in the QLM, there is no glacier distributed in the DKW, but seasonal frozen soil and snow (Lu et al., 2025).

2.2. Meteorological and soil hydrothermal observations

We established an integrated atmosphere-vegetation-soil observation system comprising four observation sites distributed along elevation gradients and vegetation types in the DKW. The characteristics for the four sites are shown in Table 1. Meteorological data including precipitation, air temperature, total solar radiation, photosynthetically active radiation, relative humidity, wind speed and direction, and atmospheric pressure, were monitored by a HOBO U30 automatic weather station with a record interval of 30 min at each site from 2015 to 2023 (2019–2023 for shrub meadow). Soil temperature and soil water content (liquid) were monitored using Campbell CS655 sensors at various soil depths at 30-minute intervals (Figure S1). The observed data are aggregated to a daily mean, except the precipitation data, which are

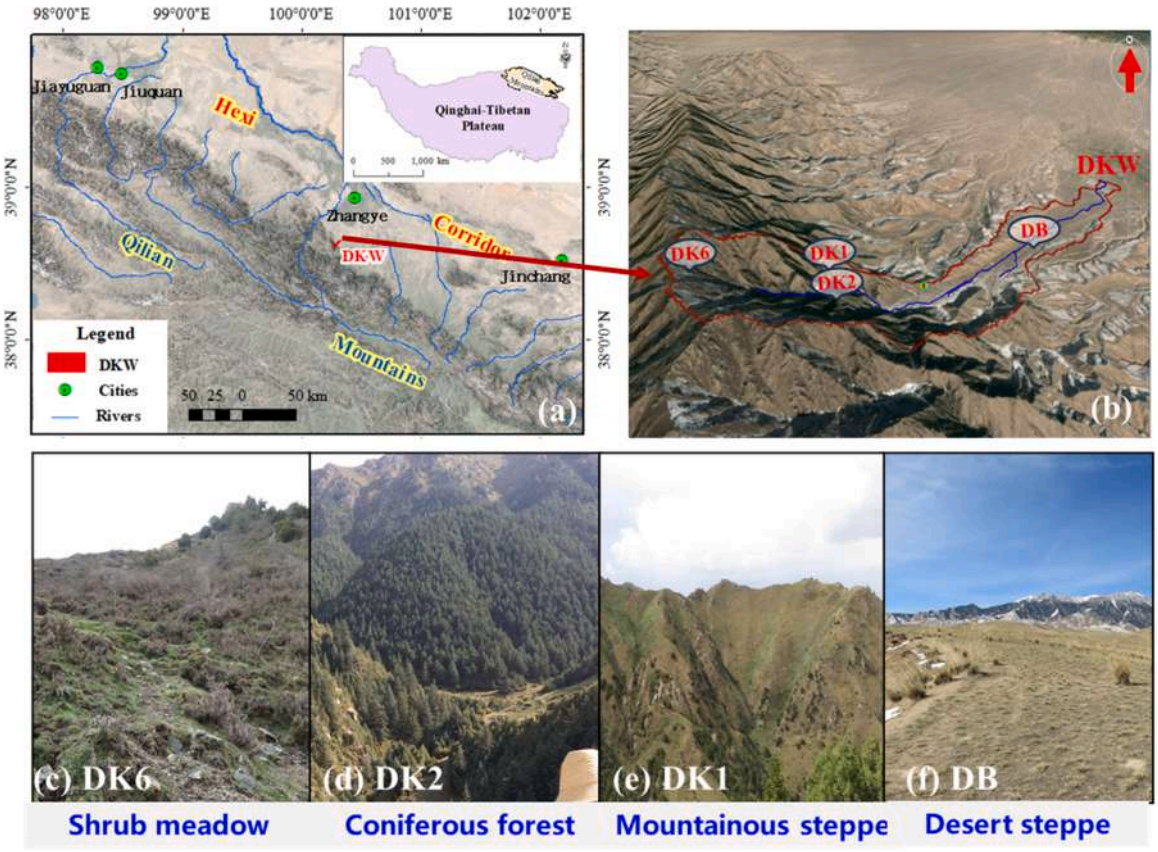

Fig. 1. Location of the Dakouzi watershed (DKW) (a), observation sites (b) and vegetation types: (c) shrub meadow (DK6), (d) coniferous forest (DK2), (e) mountainous steppe (DK1) and (f) desert steppe (DB).

Table 1
Site characteristics and soil monitoring depths in Dakouzi catchment.

Site	Elevation (m)	Aspect	Slope	Vegetation	Soil monitoring depth
DB	2300	70°	5.70°	Desert steppe	0.05 m, 0.10 m, 0.20 m, 0.40 m, 0.60 m, 0.80 m, 1.20 m, and 1.60 m
DK1	3050	180°	28.80°	Mountainous steppe	0.15 m, 0.25 m, 0.40 m, and 0.70 m
DK2	3000	0°	6.70°	Coniferous forest	0.05 m, 0.10 m, 0.20 m, 0.30 m, 0.50 m, 0.80 m, 1.00 m, and 1.40 m
DK6	3450	33°	29.70°	Shrub meadow	0.10 m, 0.25 m, 0.45 m, 0.80 m, and 1.00 m

(Aspect: degrees clockwise from due north)

summed to a daily total. These daily data were used to drive the SHAW model separately across different vegetation types.

2.3. Soil hydrothermal process modeling

2.3.1. Simultaneous heat and water (SHAW) model

The SHAW model is a one-dimensional vertical soil-vegetation-atmosphere-transfer model that simulates the surface water and energy balance, as well as the subsurface flow of heat, water, and solutes accounting for the soil freeze-thaw process (Langford et al., 2020). It considers the effects of water phase change on hydrothermal transfer processes by using the water freezing point potential equation and the soil water potential equation. The temperature distribution state equation in a frozen soil matrix including liquid convection heat transfer and latent heat of vaporization, is given as (Flerchinger and Saxton, 1989; Lu et al., 2025):

$$C_s\frac{\partial T}{\partial t}-\rho_i L_f\frac{\partial \theta_i}{\partial t}=\frac{\partial}{\partial z}\left[k_s\frac{\partial T}{\partial z}\right]-\rho_l c_l\frac{\partial q_l T}{\partial z}-L_v\left(\frac{\partial q_v}{\partial z}+\frac{\partial p_v}{\partial t}\right) \quad (1)$$

where C_s and T represent the volumetric heat capacity ($J\cdot kg^{-1}\cdot ℃^{-1}$) and temperature (℃) of the soil, respectively; ρ_i is the density of ice ($kg\cdot m^{-3}$); θ_i is the ice volume fraction ($m^3\cdot m^{-3}$); k_s is the soil thermal conductivity ($W\cdot m^{-1}\cdot ℃^{-1}$); ρ_l is the density of liquid water; c_l is specific heat capacity of water ($J\cdot kg^{-1}\cdot ℃^{-1}$); q_l is the liquid water flux ($m\cdot s^{-1}$); q_v is the water vapor flux ($kg\cdot m^{-2}\cdot s^{-1}$); and ρ_v is the density of vapor ($kg\cdot m^{-3}$).

The soil water flux under freeze-thaw conditions is simulated considering the hydraulic conductivity, matrix potential, and potential gravitational gradient in the soil, which is given as (Flerchinger and Saxton, 1989):

$$\frac{\partial \theta_l}{\partial t}+\frac{\rho_i}{\rho_l}\frac{\partial \theta_i}{\partial t}=\frac{\partial}{\partial z}\left[K\left(\frac{\partial \varphi}{\partial z}+1\right)\right]+\frac{1}{\rho_l}\frac{\partial q_v}{\partial z}+U \quad (2)$$

where K is the unsaturated hydraulic conductivity ($m\cdot s^{-1}$); φ is the soil matrix potential (m); and U is the source/sink term for water flux ($m^3\cdot m^{-3}\cdot s^{-1}$). The simulation of φ is given as (Flerchinger and Saxton, 1989):

$$\varphi=\varphi_e\left(\frac{\theta_l}{\theta_s}\right)^{-b} \quad (3)$$

where φ_e is the air entry potential (m); b is the pore size distribution parameter, and θ_s and θ_l are the saturated and liquid water content ($m^3\cdot m^{-3}$), respectively.

The initial distributions of soil temperature and moisture were both based on observations. The lower boundary condition for both water flow and heat transport were set as real-time observed soil moisture content and soil temperature in order to control the water budget in the bottom. Bulk density and particle size composition of each soil layer were determined in the laboratory using soil samples taken from the observation sites. Soil texture was determined using a laser particle size analyzer, soil bulk density was measured using the drying method, soil saturated water conductivity was measured using the fixed water head method, soil water characteristic curves were determined using a centrifuge, and the calibration of saturated water content was based on the soil water characteristic curve fitting software (Tian et al., 2017). The air entry potential φ_e and pore size distribution parameter b were adjusted based on soil bulk density and particle size composition (Lu et al., 2025) as well as the sensitivity of soil water content and soil moisture to φ_e and b (Figure S2-S5). All measured soil parameters are listed in Table S1. And the confidence interval of parameters φe and b are listed in Table S2.

2.3.2. Division of freeze-thaw periods

We defined that the whole freeze-thaw periods could be divided into four stages: freezing, completely frozen, thawing and completely thawed. Based on soil temperature observations data, we used 0°C as the critical threshold for stage identification. The freezing stage starts when surface soil temperature declines below 0 ℃ and lasts until the temperatures of all soil layers fall below 0 ℃; the completely frozen stage is the period when the temperature of all soil layers are below 0 ℃ and lasts until the surface soil temperature starts to rise above 0 ℃; the thawing stage is when the surface soil temperature starts to rise above 0 ℃ and lasts until the temperatures of all soil layers rise above 0 ℃; and the completely thawed stage is from the end of the thawing period to the beginning of the next freezing period (Gao et al., 2020). After the division stages, the rationality of the freeze-thaw periods division is verified by combining the liquid water and the solid water content data output by the SHAW model. Specifically, when the soil begins to enter the freezing stage, the content of liquid water starts to decrease, and solid water begins to appear and gradually increases. When the soil begins thawing, the content of solid water starts to decrease. When the soil is completely thawed, the solid water completely disappears.

2.3.3. Model performance assessment

The performance of the SHAW model was evaluated using four statistical metrics: the determination coefficient (R^2) (Yang et al., 2017), Nash-Sutcliffe efficiency coefficient (NSE) (Nash and Sutcliffe, 1970), root mean square error (RMSE) (Wang et al., 2023b) and confidence interval (CI) of error. The expression for the confidence interval (CI) of error is given by Lu et al. (2025):

$$CI = \overline{X} \pm t_{\frac{\alpha}{2}}(N-1)\frac{S_d}{\sqrt{N}} \quad (4)$$

Where $\overline{X}$ is the average of error, $t_{\frac{\alpha}{2}}(N-1)$ is the threshold of the t-distribution with freedom degree of n - 1, S_d is the standard deviation, and N is the amount of data. An optimal model performance is indicated by R^2 and NSE values approaching 1, and RMSE and CI values approaching 0. Conversely, unsatisfactory metric values may indicate a need to adjust

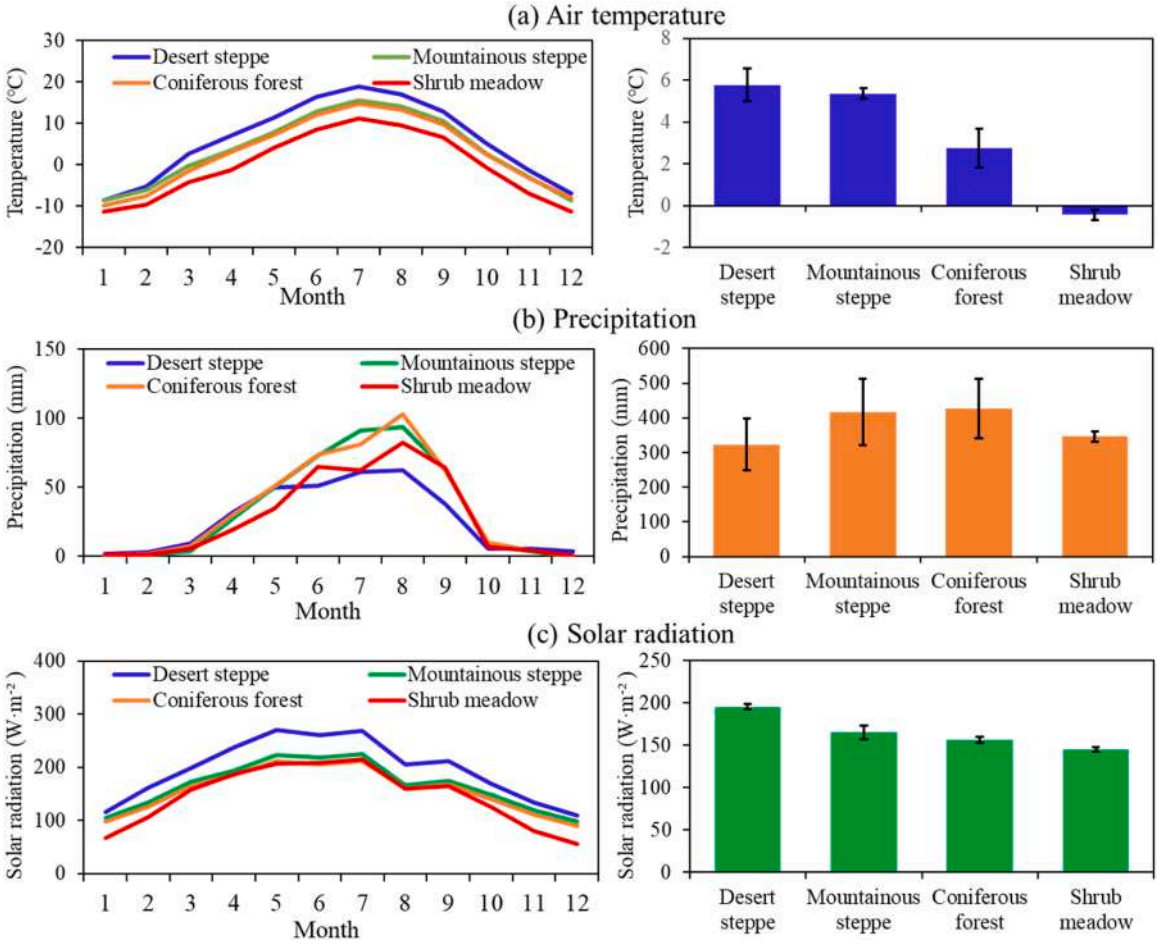

Fig. 2. Monthly (line graphs) and annual (bar graphs) average air temperature (a), precipitation (b), and solar radiation (c) from 2015 to 2023 (2019–2023 for shrub meadow) for different vegetation types in DKW. The error bar indicates the standard deviation.

the model's parameters or structure to improve simulation accuracy.

3. Results

3.1. Dynamics of observed air temperature, precipitation, soil moisture and soil temperature

Meteorological data such as air temperature, precipitation, and solar radiation from 2015 to 2023 (2019–2023 for shrub meadow) in the DKW exhibited distinct seasonal patterns (Fig. 2). From April to September, precipitation accounted for 91 %, 97 %, 94 %, and 95 % of the annual total at the desert steppe, mountainous steppe, coniferous forest, and shrub meadow, respectively. Temperature peaked in July and maximum precipitation was in August for all sites, with reduced solar radiation in August attributable to cloud cover due to the maximum precipitation. Clear elevational gradients emerged for temperature and solar radiation. Annual mean temperature decreased from 5.77 $\pm$ 0.78°C (desert steppe, 2300 m) to -0.43 ± 0.24°C (shrub meadow, 3450 m), while solar radiation declined from 195.46 $\pm$ 3.14 W·m^{-2} to 144.90 $\pm$ 2.65 W·m^{-2}. In contrast, annual precipitation demonstrated a unimodal pattern with elevation, with the highest at 3000 m in coniferous forest.

Fig. 3 shows the monthly average soil temperature and soil water content (SWC) at different depths for each vegetation type. For the four vegetation types, soil temperature exhibited clearly seasonal variation, with low values in winter and high values in summer. Due to the delayed transmission of temperature, the peak value of soil temperature declined with depth in the soil profile. Deep soil exhibited more stable temperature with reduced fluctuations than that of surface soil. As a result, the surface soil temperature was highest in summer while highest for the deep soil in winter. This pattern was particularly evident in coniferous forest and shrub meadow soils, where seasonal freeze-thaw processes were pronounced.

The intra-annual variation of SWC for the four vegetation types is different from that of soil temperature, which reflects a synergistic effect of hydrothermal conditions and soil properties. Generally, SWC was higher during the warm season (April to September) and lower in the cold season (October to March), with deep soil exhibiting greater SWC stability than surface soil. The monthly average SWC remained below 0.25 m^3 ·m^{-3} across all soil layers in desert steppe and mountainous steppe, while several layers in coniferous forest and shrub meadow consistently exceeded 0.30 m^3 ·m^{-3} . Due to the high evapotranspiration and low precipitation, the monthly averaged SWC in the top soil declined at first after September across all sites.

3.2. Simulation performance of SHAW

Fig. 4 shows the comparison of soil temperature simulation results with the observations for the four vegetation types. It indicated that the SHAW model effectively captures the dynamic variations in soil temperature across the four vegetation types during different stages of freeze-thaw process. Soil temperature simulation of the four vegetation types had a range of R^2 above 0.95, an average NSE of 0.90 and an average RMSE of 1.63°C (Table 2). Comparative analysis revealed that the shrub meadow had the most accurate simulation of the overall soil profile temperature. This superior performance is likely due to the relatively uniform vegetation structure in shrub meadows, whereas the more complex canopy and root structures in the coniferous forest, desert steppe, and mountainous steppe increase the uncertainty in estimating model parameters such as leaf area index (LAI) and root distribution,

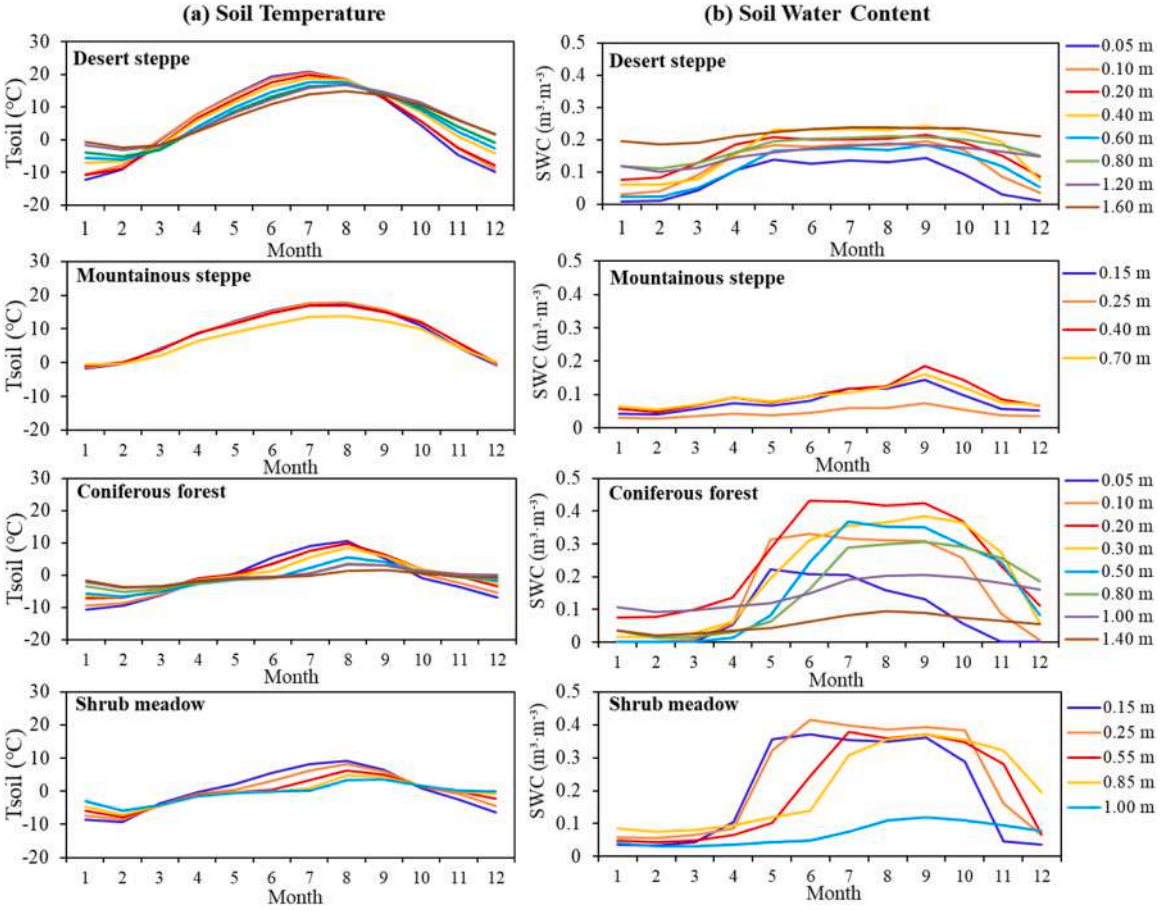

Fig. 3. Monthly average soil temperature (a) and soil water content (b) at various depths for different vegetation types in DKW.

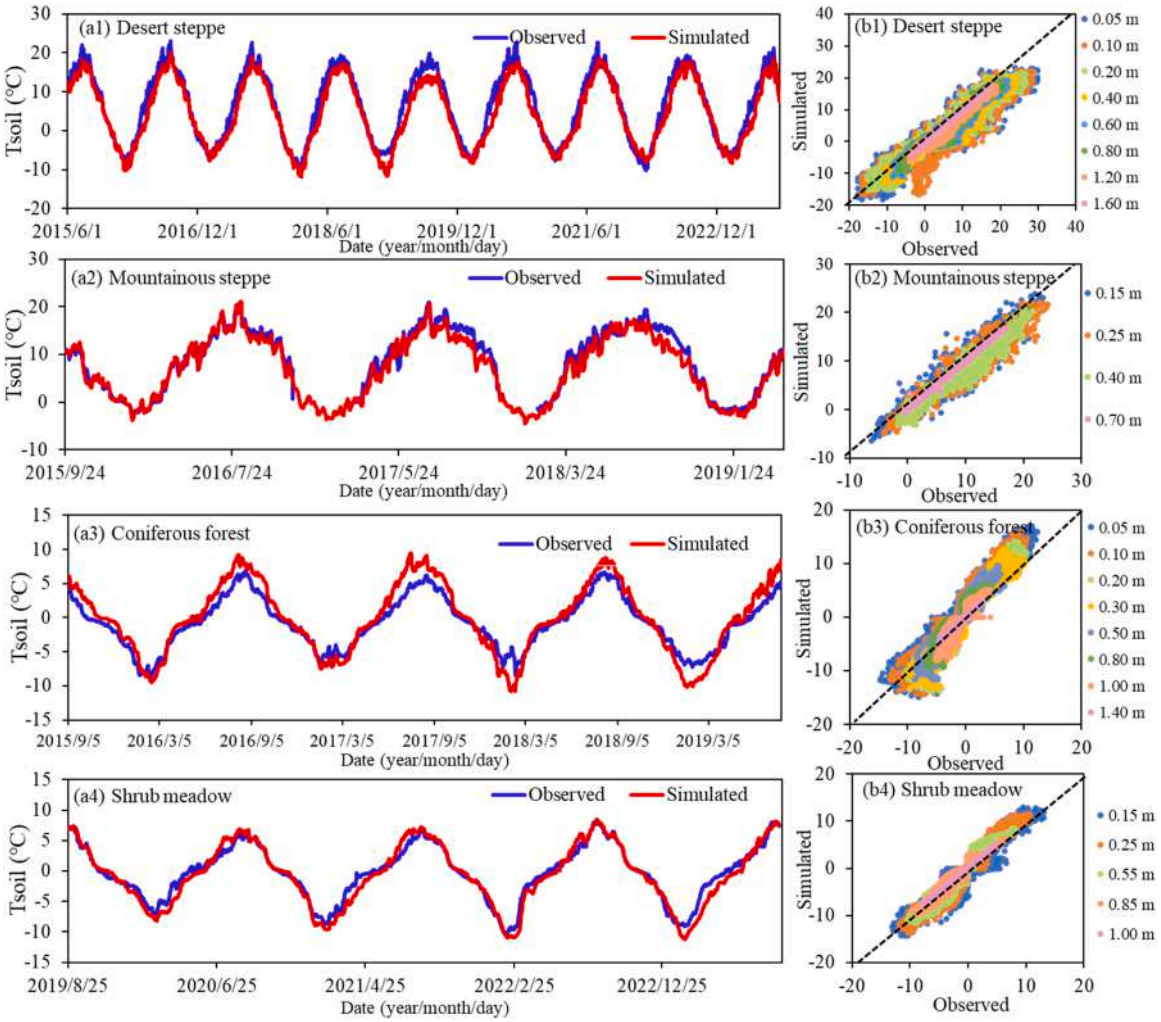

Fig. 4. Comparison of observations of daily temperature of soil profiles with those simulated by the SHAW model (a1-a4) from 2015 to 2023 (2019–2023 for shrub meadow); and scatter plots at different depths (b1-b4) for the four vegetation types in the DKW.

Table 2
Soil temperature simulation performance assessment across the four vegetation types. CI is the error metric and short for confidence interval of error.

Vegetation Types	Soil temperature			
	R^2	NSE	RMSE (°C)	CI (°C)
Desert steppe	0.96	0.93	2.43	(−1.88, −1.68)
Mountainous steppe	0.96	0.95	1.58	(−0.77, −0.64)
Coniferous forest	0.96	0.80	1.71	(0.56, 0.73)
Shrub meadow	0.97	0.93	0.79	(−0.37, −0.26)

thereby affecting simulation performance. Furthermore, the scatter plots showed stronger agreement between observed and simulated values in deep soil layers. The evaluation of soil temperature performance across various soil depths of different vegetation types is shown in Table S3. Overall, these findings demonstrate the strong correlations between simulated and measured soil temperatures across different vegetation types and soil depths, accurately capturing the dynamic soil temperature fluctuations.

Fig. 5 displayed a line graph comparing daily observed SWC across the entire profile with SHAW model simulations, while the right panel presented scatter plots of observed versus simulated values at different soil depths. The findings demonstrated that the SHAW model effectively simulated the dynamic changes in SWC across different vegetation types during the various periods of the freeze-thaw process and accurately captures frequent SWC fluctuations. For the four vegetation types, R^2 varied between 0.82 and 0.97 with an average of 0.88, NSE varied between 0.69 and 0.97 with an average of 0.86 and RMSE varied between 0.01 $m^3 \cdot m^{-3}$ and 0.04 $m^3 \cdot m^{-3}$ with an average of 0.02 $m^3 \cdot m^{-3}$ (Table 3). Among the four vegetation types, the shrub meadow exhibited the highest accuracy in SWC simulation, showing the highest R^2 and NSE, and lowest RMSE. The scatter plots in Fig. 5 revealed the SWC simulated performance of surface soil layers exhibited greater discrepancies, while deep soil layers showed strong agreement between observed and simulated values. This is likely because the precipitation-induced variability in surface SWC was more profound. The evaluation of SWC performance across various soil depths of different vegetation types is shown in Table S4. Comparative analysis indicated that soil temperature simulations were more accurate than that of soil moisture across the four vegetation types.

3.3. Characteristics of the soil freeze-thaw process

The duration of freeze-thaw stages varied significantly among vegetation types due to differences in elevation and slope aspect (Fig. 6). All four vegetation types exhibited relatively brief freezing and thawing stages (<80 days), with the mountainous steppe showing the shortest durations (33 and 28 days, respectively). Although the air temperature and solar radiation is highest for the desert steppe, the duration of the completely frozen stage is not the shortest nor the longest for the

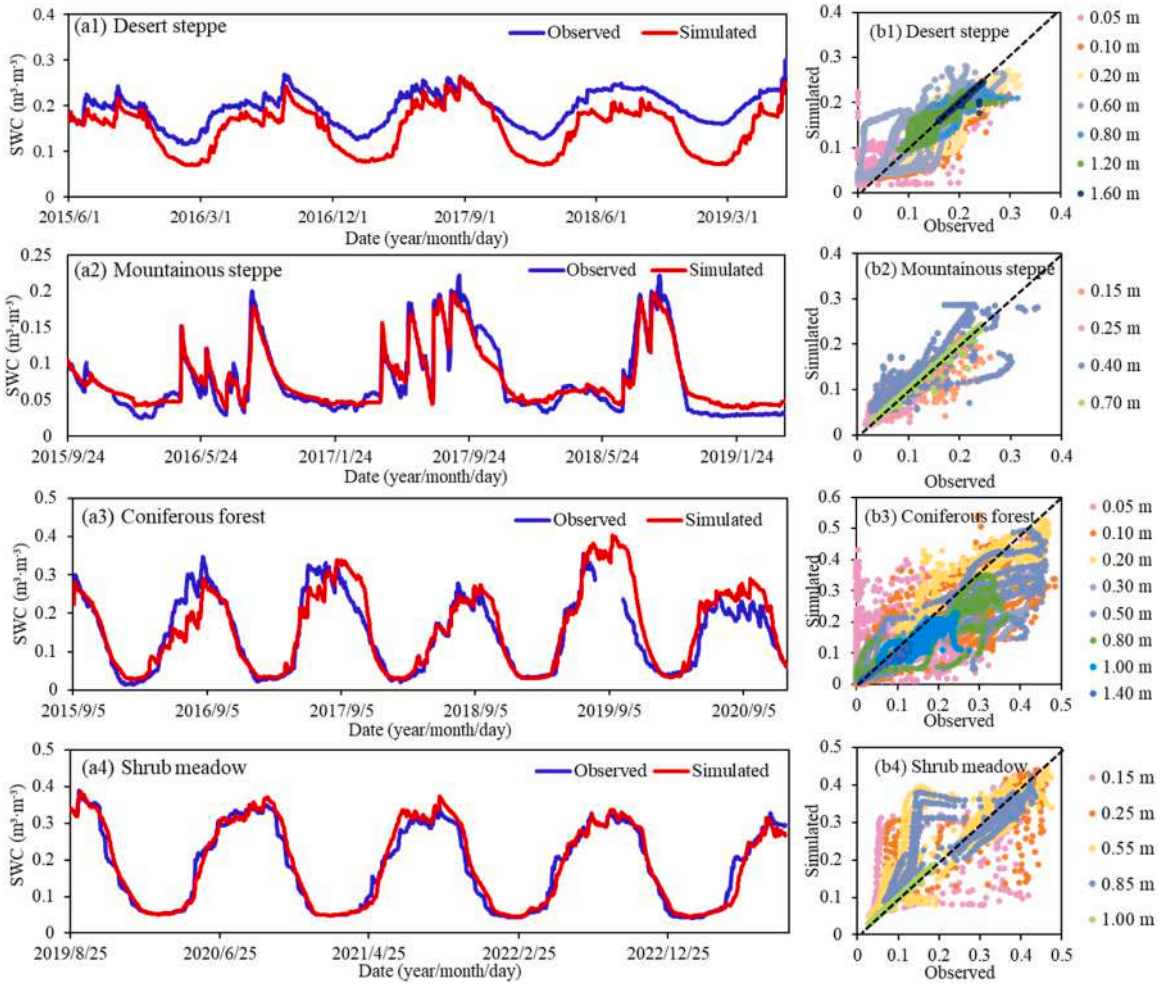

Fig. 5. Comparison of observed daily soil water content (SWC) of soil profiles with those simulated by the SHAW model (a1-a4) from 2015 to 2023 (2019–2023 for shrub meadow) as well as scatter plots at different depths (b1-b4) for the four vegetation types in the DKW.

Table 3
SWC simulation performance assessment across the four vegetation types. CI is the error metric and short for confidence interval of error.

Vegetation Types	Soil water content			
	R^2	NSE	RMSE ($m^3 \cdot m^{-3}$)	CI ($m^3 \cdot m^{-3}$)
Desert steppe	0.82	0.69	0.03	(−0.046, −0.043)
Mountainous steppe	0.92	0.97	0.01	(0.002, 0.003)
Coniferous forest	0.83	0.80	0.04	(0.007, 0.011)
Shrub meadow	0.97	0.96	0.01	(0.004, 0.006)

duration of the completely thawed stage. Due to its low vegetation coverage, high solar radiation and location on a sunny slope, the duration of the completely frozen stage at the mountainous steppe is the shortest (44 days), while the duration of the completely thawed stage is the longest (269 days). Although the air temperature and solar radiation for the shrub meadow were the lowest among the four vegetation types, the duration of the completely frozen stage is not the shortest. Among the four vegetation types, the longest duration of the completely frozen stage (123 days) and the shortest duration of the completely thawed stage (101 days) was at the coniferous forest.

Fig. 7 illustrated the temporal dynamics of soil temperature profiles across the four vegetation types from 2015 to 2023 (2019–2023 for shrub meadow), revealing distinct patterns of heat distribution and transfer during freeze-thaw process. The 0°C isotherm (dark red line) marks the boundaries of freeze-thaw stages. During the freeze-thaw processes, each soil layer undergoes cooling-warming-cooling cycles, with soil temperature variation rates decreasing and stability increasing with depth. During the freezing and completely frozen stages, soil layers freeze progressively downward, exhibiting temperature increasing with depth across four vegetation types. Soil temperature decreased with an increase in soil depth in both thawing and completely thawed stages across the four vegetation types. A comparison of the four vegetation types revealed that soil temperature in shrub meadow and coniferous forest were lower compared to those in desert steppe and mountainous steppe during the freezing and completely frozen stage. The lowest soil profile temperature of shrub meadow and coniferous forest were −11.40℃ and −11.28℃, while the lowest soil profile temperature of the mountainous steppe and desert steppe were −3.90℃ and −10.47℃, respectively. In contrast, the soil temperature in mountainous steppe and desert steppe were higher than those of shrub meadow and coniferous forest during thawing and completely thawed stage. The maximum profile temperature was 20.83°C for mountainous steppe and 19.99°C for desert steppe, while shrub meadow and coniferous forest reached only 8.88°C and 10.61°C, respectively.

Fig. 8 illustrates variations in soil liquid water content across the soil profiles of the four vegetation types from 2015 to 2023 (2019–2023 for shrub meadow). Results revealed the soil liquid water content of soil profiles within the four vegetation types undergoes a decreasing - increasing - decreasing process, which is highly consistent with the soil freeze-thaw process. The soil liquid water content was markedly higher during thawing and completely thawed stages compared to that during

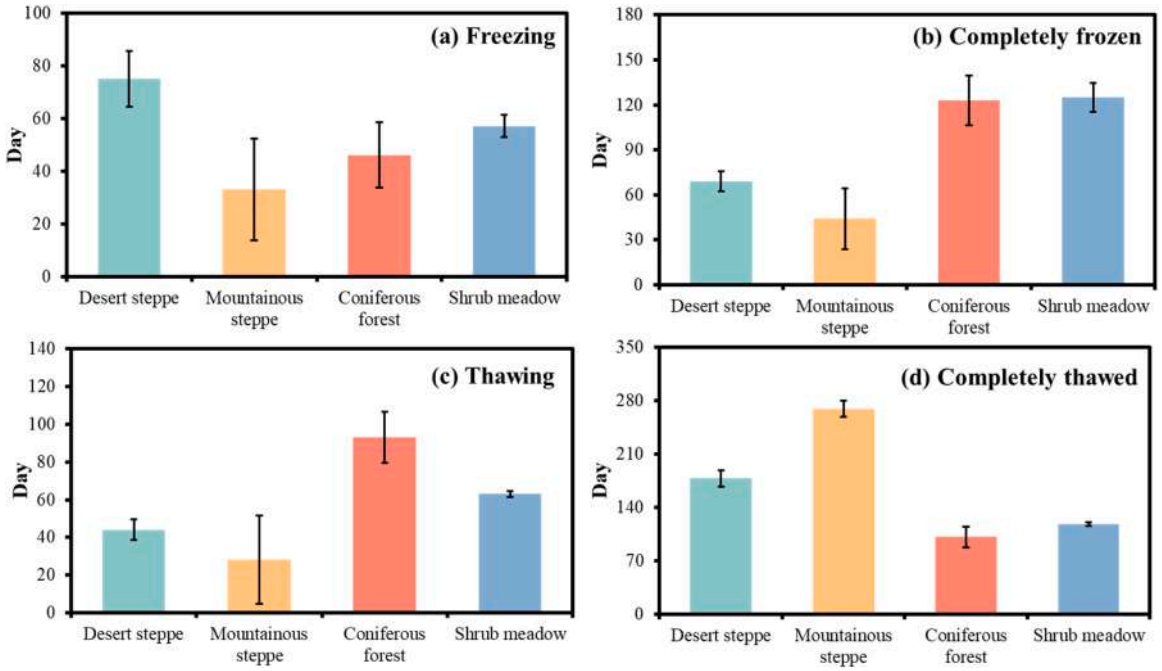

Fig. 6. Number of days for the different freeze-thaw stages (a-d) across the four vegetation types in DKW. Error bars present the standard deviation.

freezing and completely frozen stages across the four vegetation types. Furthermore, the liquid water content in the soil of shrub meadow and coniferous forest exceeds that of desert steppe and mountainous steppe during thawing and completely thawed stages. The highest liquid water content in the soil profile of shrub meadow and coniferous forest was 0.38 $m^3 \cdot m^{-3}$ and 0.42 $m^3 \cdot m^{-3}$, respectively, while in mountainous steppe and desert steppe they were 0.24 $m^3 \cdot m^{-3}$ and 0.27 $m^3 \cdot m^{-3}$. The soil liquid water distribution in the soil profiles of the four vegetation types differed: liquid water in the soil of desert steppe, mountainous steppe and shrub meadow were higher in the soil layers above a depth of 1.00 m, and lower below 1.00 m. The distribution of soil liquid water in the soil profile of shrub meadow was more uniform. The soil liquid water of the desert steppe, mountainous steppe and coniferous forest was highest at the 0.40 m depth, while in the soil of shrub meadow, it was highest at the 0.25 m depth.

Soil temperature dynamics at different soil depths for the four vegetation types at the four freeze-thaw stages showed significant differences (Fig. 9). We can see the variation of soil moisture and soil temperature in different freeze-thaw stages was significantly different across the four vegetation types, and significantly different only for soil moisture in different vegetation types across the four phases. Because the four freeze-thaw phases were defined by soil temperature, the difference for soil temperature in different vegetation types was insignificant across the four phases (Table S5). During the freezing stage, temperature increased nonlinearly when depth increased. The deepest layer reached 0°C for all vegetation types except the desert steppe, where it remained above 0 ℃. For the top soil, the soil temperature for the coniferous forest is the highest, while that of the desert steppe is the lowest. During the completely frozen and completely thawed stages, the soil temperature dynamics linearly increased with the soil depth rising. During the completely frozen stage, the desert steppe had the lowest profile-wide temperatures, followed by the shrub meadow and coniferous forest. During the completely thawed stage, the soil temperature over the whole profile for the shrub meadow was the lowest, followed by coniferous forest and mountainous steppe, and was highest for the desert steppe with the mean soil temperature reaching to 12 ℃. During thawing stage, soil temperature showed a nonlinear decrease and then increased with soil depth rising for the four vegetation types, especially in desert steppe. The dynamics of soil temperature during the four freeze-thaw stages indicated that the soil froze from top to bottom, and thawed from both directions.

Progressive top-down soil freezing, with delayed freezing timing and increased unfrozen water content at greater depths in the study area was seen. However, soil water content (SWC) displayed spatiotemporal heterogeneity across depths, influenced by temperature dynamics, precipitation, vegetation uptake, and soil properties (Fig. 9). SWC profiles of the four vegetation types showed clear differences across every freeze-thaw stages. However, for each vegetation type, the SWC profiles were similar across the four freeze-thaw stages. The average SWC of soil profile across all stages for the mountainous steppe was lowest in comparison with the other three vegetation types with a SWC below 0.1 $m^3 \cdot m^{-3}$, due to its relatively high radiation and evapotranspiration. Compared to the other three stages, the completely frozen stage had the lowest SWC for all vegetation types at a value below 0.1 $m^3 \cdot m^{-3}$ for most soil layers. The SWC in the middle layers (*e.g.* 20 cm to 60 cm) was relatively high and had a large amplitude, especially in thawing and completely thawed stages, indicating that the potential water storage was large at these depths.

3.4. Runoff regime and water balance in different freeze-thaw stages

Based on the results of the SHAW model, we calculated the average daily processes of water flux as well as accumulative water fluxes from the daily values (Fig. 10). For all four vegetation types, precipitation and evapotranspiration primarily occurred in summer and autumn, with soil moisture dynamics responding to precipitation events greater than 5 mm. However, there were distinct differences in terms of runoff and deep seepage across different vegetation types. There was almost no surface runoff formed in desert steppe and mountainous steppe, and deep seepage was also small but had great variability for soil moisture in correspondence to precipitation. Because the soil of mountainous steppe is generally thin, only a small amount of rainfall could be held in the soil during the rainy season. Similarly, the coniferous forest exhibited no deep seepage, primarily due to rainfall interception by the understory (especially moss), which stored water at the surface and impeded deep infiltration. In contrast, the coniferous forest and shrub meadow exhibited notable surface runoff during the thawing stage, especially for shrub meadow. Since the soil is still frozen when the snow begins to

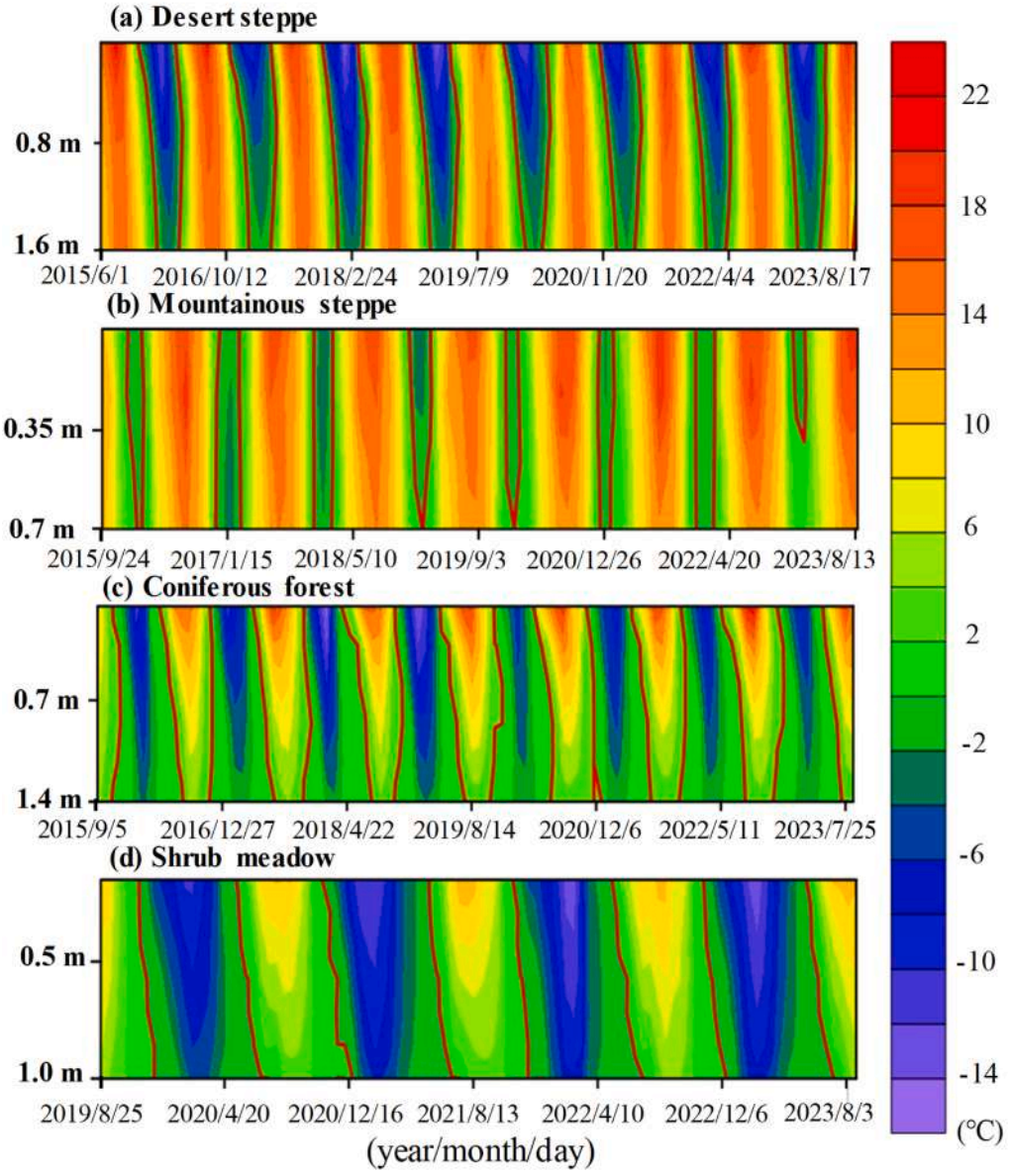

Fig. 7. Soil temperature dynamics along the soil profiles for the four vegetation types (a-d) in the DKW from 2015 to 2023 (2019–2023 for shrub meadow). The dark red line represents 0°C isotherm.

thaw, snowmelt gathers on the surface to form surface runoff rather than infiltrating into the soil. As the thawing stage continues, the soil begins to thaw from the surface to deep soil. The soil's ability to conserve water is enhanced, and the snowmelt, therefore, infiltrates into the soil. Thus, surface runoff was mainly generated in the early thawing stage. It is worth noting that, unlike the other three vegetation types, there was obvious deep seepage in the soil of shrub meadow, with an annual deep seepage volume reaching 116.56 mm. This may be due to a strong infiltration capacity in the soil of shrub meadow. According to the soil characteristic parameters in Table S1, the saturated water conductivity (K_S) of the shrub meadow soil is significantly higher than that of the other three vegetation types. In addition, the soil layer of the shrub meadow is relatively thin and thus it is prone to deep seepage formation. This seepage, emerging as baseflow, has become an important source of streamflow in this region. Water flux accumulation curves showed precipitation concentrated from April to September with evapotranspiration consuming the most. Coniferous forest experienced summer soil moisture deficits when evapotranspiration exceeded precipitation in the growth season, while other vegetation types showed seasonal soil moisture fluctuations.

The statistics of water fluxes for different vegetation types showed distinct hydrological behaviors in different freeze-thaw stages (Fig. 11). During the freezing and completely frozen stages, the water fluxes of all vegetation types are relatively small. However, due to air temperatures above 0 ℃ for parts of some days, the snow began to thaw while the surface soil was still frozen and there was a small amount of surface runoff formed in coniferous forest and shrub meadow, where the snowfall was larger than that in desert steppe and mountainous steppe. During the thawing and completely thawed stages, with an increase in precipitation, water fluxes began to rise, especially evapotranspiration. In the completely thawed stage, evapotranspiration accounted for 93 %, 94 %, 81 %, and 62 % of the precipitation in the desert steppe, mountainous steppe, coniferous forest, and shrub meadow, respectively. It should be noted that for desert steppe and mountainous steppe, the evapotranspiration is dominated by soil evaporation, which accounts for 79 % and 92 % of total evapotranspiration, respectively. In coniferous

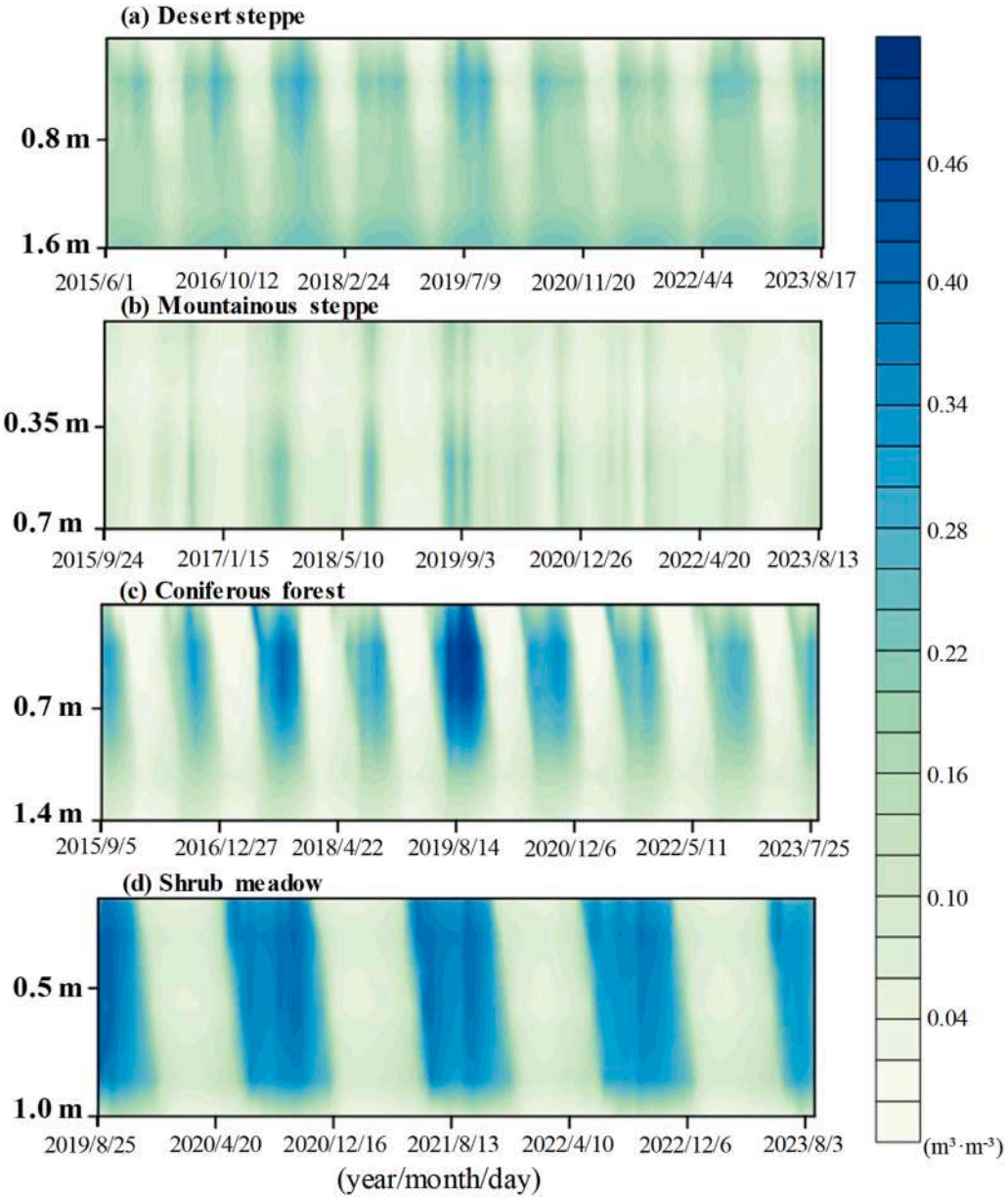

Fig. 8. Soil water content (liquid water) dynamics along the soil profiles for the four vegetation types (a-d) in DKW from 2015 to 2023 (2019–2023 for shrub meadow).

forest and shrub meadow, the evapotranspiration is dominated by vegetation transpiration, which accounts for 59 % and 78 % of total evapotranspiration, respectively. The reason for this difference is the vegetation of coniferous forest and shrub meadow is obviously higher than that of desert steppe and mountainous steppe. Specifically, the leaf area index of coniferous forest and shrub meadow is 1.1 and 2.5, while that of desert steppe and mountainous steppe it is only 0.1 and 0.8, respectively. Furthermore, the coniferous forest and shrub meadow were located on shady slopes at high elevation, and the thawing stage started later than that of desert steppe and mountainous steppe; meanwhile, the soil profile was still frozen when the snow began to melt in the early thawing stage. Therefore, there was surface runoff formed in coniferous forest and shrub meadow in this stage. The shrub meadow has a large capacity of rainfall redistribution and infiltration in the completely thawed stage; there was a distinct deep seepage in this stage that could became a major source of recharge to streamflow.

4. Discussion

4.1. Spatial heterogeneity of the soil freeze-thaw process

The spatial heterogeneity of the soil freeze-thaw process refers to variations in the occurrence, intensity, and impact of soil freezing and thawing across different locations within a given area. This phenomenon is influenced by numerous factors, including soil types, vegetation cover, topography, and climatic conditions (Ala et al., 2016; Bo et al., 2021; Chen et al., 2013; Iwata et al., 2008; Sun et al., 2021; Wang et al., 2019a). In this study, observation sites under different vegetation types and altitudes were selected to analyze the heterogeneity of the soil freeze-thaw process. The results showed that the start of freezing was the earliest and thawing was the latest in coniferous forest, while the start of freezing was the latest and thawing was the earliest in mountainous steppe among the four vegetation types. As a result, the average duration of completely frozen stage was the longest in coniferous forest and the shortest in mountainous steppe (Figs. 6 and 9). This discrepancy can be

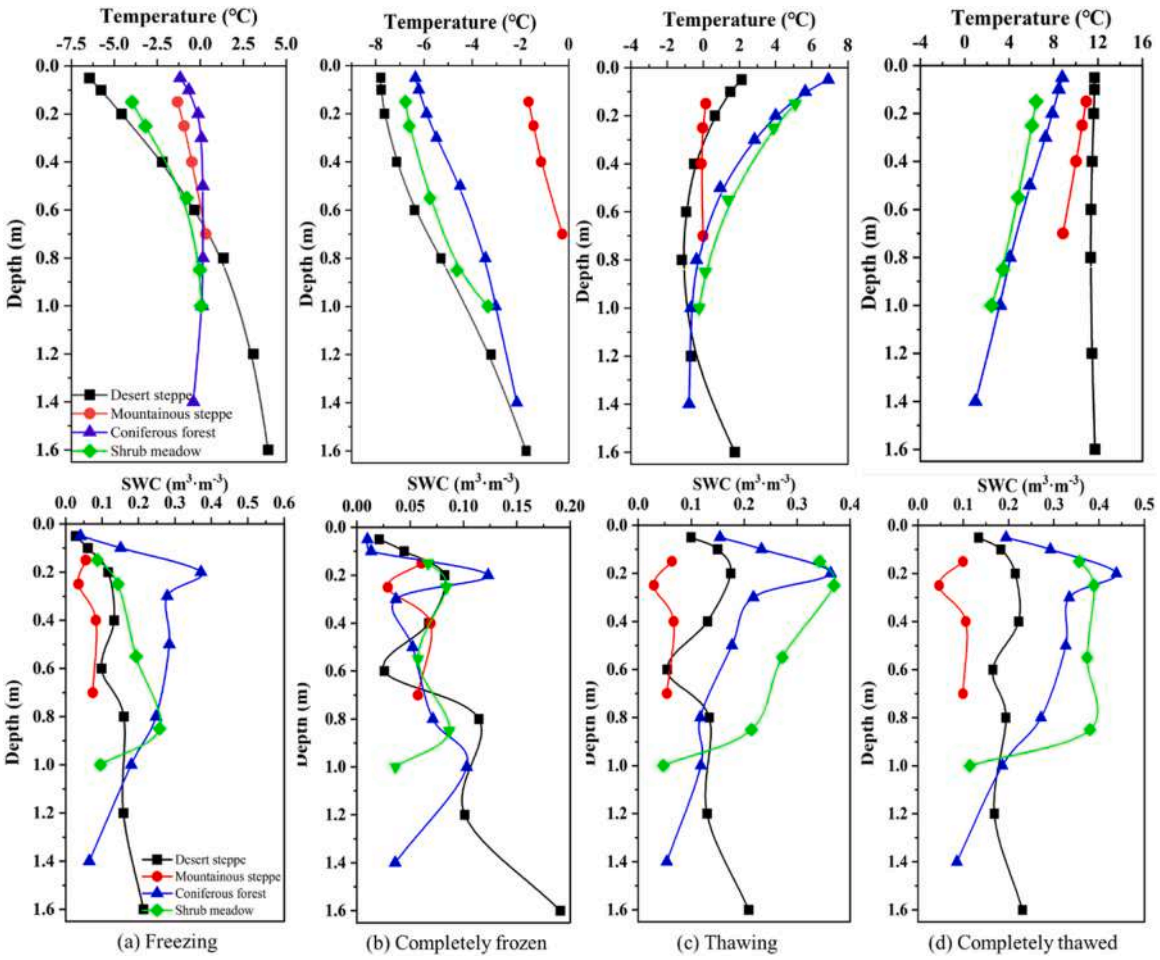

Fig. 9. Average soil temperature and soil water content (liquid water) dynamics with soil depth at different freeze-thaw stages (a-d) across the four vegetation types in the DKW.

primarily attributed to the fact that the mountainous steppe is located on a sun-exposed slope with sparse vegetation coverage, lacking canopy shading effects, which results in the soil receiving more solar radiation and consequently accelerating the thawing process. In contrast, the dense canopy of the coniferous forest could reduce the amount of solar radiation reaching the soil surface, thereby cooling the soil, and delaying the freeze-thaw processes. These findings are consistent with previous studies (Chasmer et al., 2011; Shur and Jorgenson, 2007). Furthermore, dense vegetation can isolate the soil, reducing the depth and intensity of soil freezing, while sparse vegetation can expose the soil to be more sensitive to surface temperature and solar radiation variations, leading to more deep and intense freeze-thaw processes (Wang et al., 2023a). Our research has confirmed that even in high-altitude areas, the thawing time of coniferous forest soil is significantly longer than that of shrub meadow soil (Fig. 6). This is likely due to the insulating effect of the fallen leaves accumulated on the surface of coniferous forest soil, which prolongs the melting time. Therefore, the heterogeneity of soil freeze-thaw characteristics largely depends on the differences in vegetation types as well as topography such as slope aspect and elevation, which could result in hydrothermal variation.

Existing studies indicate that, in addition to vegetation and slope aspect, higher altitude generally leads to an earlier onset of freezing and a later onset of thawing (Li et al., 2012; Peng et al., 2016; Wang et al., 2015). However, in this study, the freeze-thaw period of mountainous steppe at an altitude of 3050 m was shorter than that of the desert steppe at an altitude of 2300 m. The reason for this difference is very likely that mountainous steppe is located on sunny slopes where the desert steppe is sparse and thus receives more solar radiation. Therefore, in this specific situation, the influence of vegetation type and aspect on soil freeze-thaw dynamics seems to exceed that of altitude.

What is worth further exploration is that, under the current context of climate warming, the dynamics of soil freeze-thaw may undergo corresponding changes. If the temperature continues to rise in the future, leading to the start of soil freezing to be delayed and the thawing process to be accelerated, thereby shortening the overall freeze-thaw processes, especially in high-altitude and sparsely vegetated areas, it will be more sensitive. Vegetation acts as a key buffer, where differences in types and structures regulate the intensity of this climate response. For instance, dense-canopy types like coniferous forests can mitigate the thermal shock of air temperature fluctuations on soil, whereas sparsely vegetated areas are more vulnerable to climate change impacts. Therefore, in future research, it is necessary to couple climate scenarios with surface parameters to further reveal the evolution of the freeze-thaw mechanism under the interaction of multiple factors, providing a theoretical basis for the prediction and management of ecological hydrological processes in cold regions.

4.2. Impact of the soil freeze-thaw process on the runoff generation

The runoff regime refers to the process and underlying factors that govern the generation of different runoff components. The soil freeze-thaw process significantly influences the runoff generation mechanism by altering soil properties and moisture states (Connon et al., 2014; Wang et al., 2017). Our results revealed the runoff generation in the study area present large differences among different freeze-thaw stages and vegetation types. During the freezing and the completely thawed

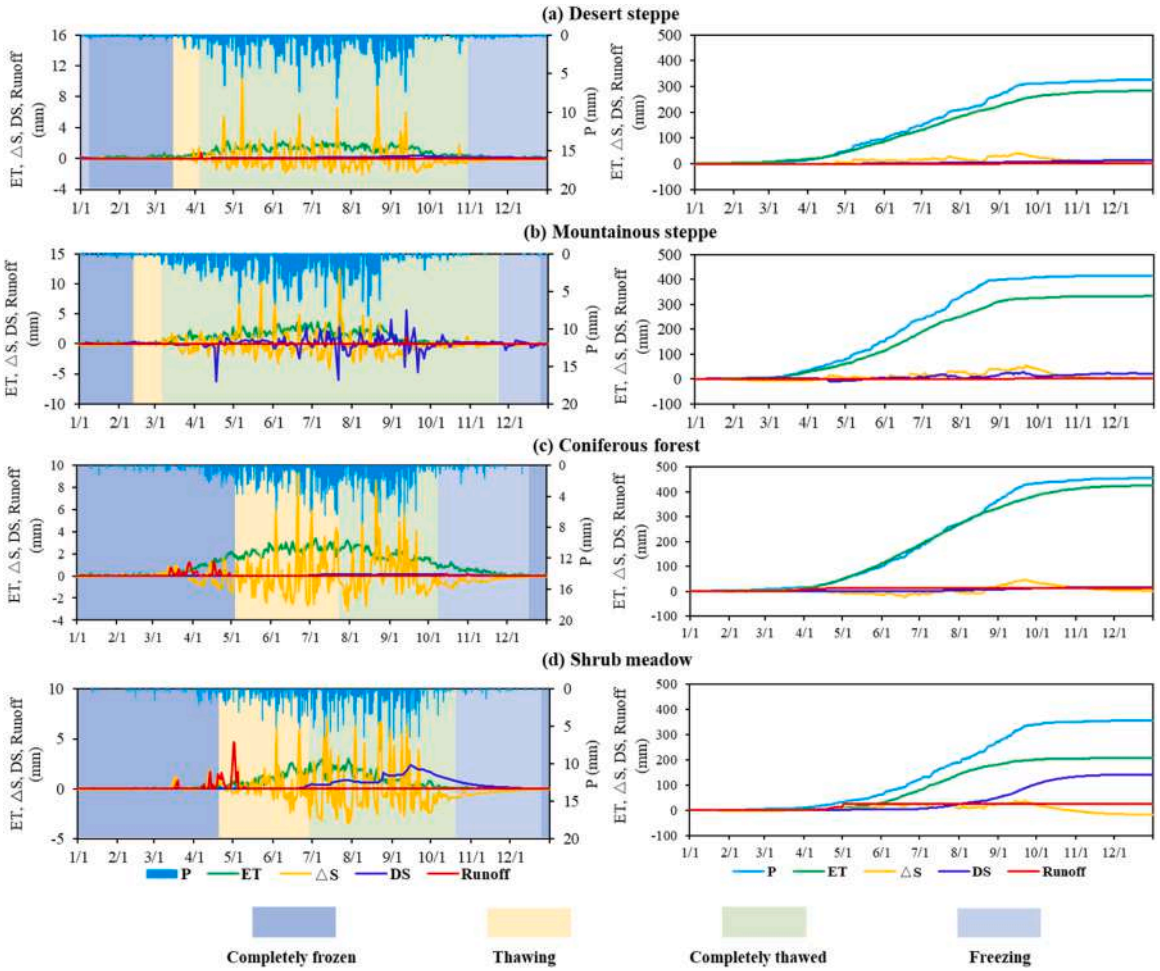

Fig. 10. Averaged daily processes (left) and accumulation (right) of averaged daily water fluxes from 2015 to 2023 (2019–2023 for shrub meadow) for different vegetation types (a-d) in the DKW. P: Precipitation, ET: Evapotranspiration, ΔS: Soil water variation, DS: Deep seepage, R: Runoff.

stages, due to the unfrozen deeper soil and its strong permeability, the amount of deep seepage is relatively larger, especially in shrub meadow (24.61 mm and 89.29 mm, respectively), in comparison with the surface runoff. Therefore, the main runoff generation mechanism of this region in these periods is the discharge of sub-surface flow by deep seepage from shrub meadow, which is consistent with the research of Cheng et al. (2024). During the completely frozen stage, water crystallization within soil pores modifies the soil's physical structure and hydraulic properties (Rooney et al., 2022). As liquid water transitions into ice, expansion displaces soil particles, reducing porosity and permeability (Ming et al., 2022). These changes diminish unfrozen water content and impede infiltration (Zheng et al., 2023), as a result, there is relatively small deep seepage and soil water storage variation during this stage (Figs. 10 and 11). Additionally, precipitation during this stage and the early thawing stage predominantly occurred as snowfall, and was relatively larger in coniferous forest and shrub meadow. Meanwhile, due to the limited soil thawed depth, the snowmelt cannot fully infiltrate in the early thawing stage, therefore, the runoff generation mechanism of this region in the completely frozen stage and thawing stage is mainly surface runoff generation from coniferous forest and shrub meadow.

This study provides a quantitative analysis of precipitation partitioning, revealing evapotranspiration as the dominant pathway for water loss in the watershed. Evapotranspiration accounted for 93 %, 94 %, 81 %, and 62 % of precipitation in the desert steppe, mountainous steppe, coniferous forest, and shrub meadow, respectively. This gradient underscores the controlling influence of vegetation on the hydrological regime. The steppe systems were characterized by a high evapotranspiration ratio, whereas the shrub meadow and coniferous forest retained greater runoff potential due to their strong canopy interception, high litter layer water-holding capacity, and surface conditions more conducive to runoff generation. These water redistribution mechanisms, combined with precipitation differences of elevation gradient, directly shaped the distinct runoff responses of each vegetation type. Therefore, no surface runoff occurred in the mountainous steppe and desert steppe. In contrast, surface runoff in the coniferous forest and shrub meadow was primarily generated during the completely frozen stage and thawing stage, with the shrub meadow yielding the highest surface runoff among all types (Fig. 11). Under global warming conditions, the freezing stage in the seasonal permafrost area is delayed and the thawing period is advanced, thereby changing the regional hydrological process. The shortening of the freeze-thaw processes at high altitudes may reduce winter surface runoff, while enhancing deep seepage and baseflow recharge.

4.3. Limitations

In this study, we simulated the soil temperature and moisture dynamics at four observations sites based on the SHAW model, and revealed the runoff formation mechanism under different freeze-thaw stages. There are still some uncertainties that need to be further optimized and verified in future studies. Firstly, the soil parameters in the model, such as air entrance potential energy (φ_e) and pore distribution parameters (b), are mainly determined based on relevant literature or sensitivity analysis, rather than calibrated based on in-site

Fig. 11. Averaged water flux from 2015 to 2023 (2019–2023 for shrub meadow) during different freeze-thaw stages (a-d) across different vegetation types in DKW. P: Precipitation, ET: Evapotranspiration, Tc: Transpiration, ΔS: Soil water variation, DS: Deep seepage.

measurement, which may affect the accuracy of simulation results to some extent. Secondly, the treatment of vegetation features in SHAW model is relatively simple, and the dynamic of vegetation as well as spatial heterogeneity effects on soil water and heat conditions are not fully considered. Moreover, the meteorological elements (such as temperature and precipitation) used as model driving data themselves have observation or interpolation errors, which will further affect the reliability of the simulation results. To improve the accuracy and robustness of SHAW model in simulating the soil water and heat process under freeze-thaw conditions, more accurate field observation and soil sampling are necessary to optimize the calibration of key parameters. In terms of future climate change, research should focus on long-term monitoring networks, basin-scale runoff assessment, and the incorporation of regional hydrological models with a freeze-thaw module to improve the understanding of runoff generation and water balance in alpine regions.

5. Conclusions

The soil freeze-thaw processes exert a profound influence on the runoff mechanism. In this study, the SHAW model was applied to an integrated atmosphere-vegetation-soil observation system along different elevations and vegetation types to investigate the spatial heterogeneity of the soil freeze-thaw process in different landscapes, and reveal the runoff regimes during different freeze-thaw stages. The following conclusions were drawn:

1. The SHAW model effectively captures the dynamic variations in soil temperature and soil moisture across different vegetation types in an alpine region during different stages of the freeze-thaw process, especially for soil temperature.
2. The length of each freeze-thaw stage for the four vegetation types showed notable differences due to the varying elevations and aspects. The average water content (liquid water) increased with soil depth. When comparing across different vegetation types, shrub meadow and coniferous forest exhibit lower soil temperature and higher moisture. In contrast, mountainous steppe and desert steppe display higher soil temperature and lower moisture.
3. There are significant differences in runoff and deep seepage among different vegetation types. There is almost no surface runoff formation in desert steppe and mountainous steppe, and the deep seepage is also slight. Unlike the other three vegetation types, the shrub meadow formed a deep seepage of 89.29 mm during the completely thawed stage, becoming the main source of runoff recharge. Affected by the freeze-thaw processes, more than 67 % of deep seepage occurs in the completely thawed stage, and more than 93 % of surface runoff occurs in the completely frozen and thawed stages. Evaporation and transpiration mainly occur in the thawing and completely thawed stages. In desert steppe and mountainous steppe, soil evaporation is dominant, while in coniferous forest and shrub meadow, vegetation transpiration is dominant. These results can be used to predict regional streamflow and available water volume more accurately, and provide information for integrated water resources management practices to ensure the sustainable utilization of water resources in alpine areas.

CRediT authorship contribution statement

Qi Feng: Writing – review & editing, Visualization, Supervision,

Conceptualization. **Honghua Xia:** Visualization, Validation, Formal analysis, Data curation. **Raffaele Albano:** Writing – review & editing, Validation, Software, Resources. **Bogdan Ozga-Zielinski:** Writing – review & editing, Visualization, Validation. **Jan Adamowski:** Writing – review & editing, Visualization, Validation, Software. **Jingru Wang:** Visualization, Validation, Software, Resources, Data curation. **Tiaoxue Lu:** Writing – review & editing, Methodology, Investigation, Funding acquisition, Formal analysis, Data curation. **Wanghan He:** Validation, Software, Methodology, Investigation, Formal analysis. **Xingyi Zou:** Software, Resources, Methodology, Investigation. **Linshan Yang:** Writing – review & editing, Writing – original draft, Visualization, Software, Resources, Project administration, Methodology, Funding acquisition, Formal analysis, Conceptualization.

Declaration of Competing Interest

The authors declare that they have no known competing financial interests or personal relationships that could have appeared to influence the work reported in this paper.

Acknowledgments

This paper was supported by the National Natural Science Fund of China (Grant No. 52522901, 52379030), the Strategic Priority Research Program of CAS (Grant No. XDB0720202), the Gansu Provincial Science and Technology Planning Project (Grant No. 24JRRA079), and the Youth Innovation Promotion Association of CAS (Grant No. 2022435). The authors appreciate the reviewers and editors for their valuable comments and suggestions.

Appendix A. Supporting information

Supplementary data associated with this article can be found in the online version at doi:10.1016/j.agwat.2026.110191.

Data availability

Data will be made available on request.

References

Ala, M.S., Liu, Y., Wang, A.Z., Niu, C.Y., 2016. Characteristics of soil freeze–thaw cycles and their effects on water enrichment in the rhizosphere. Geoderma 264, 132–139. https://doi.org/10.1016/j.geoderma.2015.10.008.

Bo, L.F., et al., 2021. Soil freeze-thaw and water transport characteristics under different vegetation types in seasonal freeze-thaw areas of the Loess Plateau. Front. Earth Sci. 9. https://doi.org/10.3389/feart.2021.704901.

Chasmer, L., Quinton, W., Hopkinson, C., Petrone, R., Whittington, P., 2011. Vegetation Canopy and Radiation Controls on Permafrost Plateau Evolution within the Discontinuous Permafrost Zone, Northwest Territories, Canada. Permafr. Periglac. Process. 22 (3), 199–213. https://doi.org/10.1002/ppp.724.

Chen, H., et al., 2015. Noah modelling of the permafrost distribution and characteristics in the West Kunlun Area, Qinghai-Tibet Plateau, China. Permafr. Periglac. Process. 26 (2), 160–174. https://doi.org/10.1002/ppp.1841.

Chen, R., et al., 2018. Effects of cryospheric change on alpine hydrology: combining a model with observations in the upper reaches of the Hei River, China. J. Geophys. Res. Atmos. 123 (7), 3414–3442. https://doi.org/10.1002/2017JD027876.

Chen, S., Ouyang, W., Hao, F., Zhao, X., 2013. Combined impacts of freeze-thaw processes on paddy land and dry land in Northeast China. Sci. Total Environ. 456-457, 24–33. https://doi.org/10.1016/j.scitotenv.2013.03.059.

Cheng, Z., et al., 2024. Effect of seasonal freeze–thaw process on spatial and temporal distribution of soil water and its infiltration to recharge groundwater. Hydrol. Process 38 (3), e15110. https://doi.org/10.1002/hyp.15110.

Connon, R.F., Quinton, W.L., Craig, J.R., Hayashi, M., 2014. Changing hydrologic connectivity due to permafrost thaw in the lower Liard River valley, NWT, Canada. Hydrol. Process 28 (14), 4163–4178. https://doi.org/10.1002/hyp.10206.

Dobiński, W., 2020. Permafrost active layer. Earth-Sci. Rev. 208, 103301. https://doi.org/10.1016/j.earscirev.2020.103301.

Dong, C., et al., 2023. Effects of freeze-thaw cycles on the size distribution and stability of soil aggregate in the permafrost regions of the Qinghai-Tibetan Plateau. Environ. Res. Commun. 5 (9), 095008. https://doi.org/10.1088/2515-7620/acf651.

Flerchinger, G., Saxton, K., 1989. Simultaneous heat and water model of a freezing snow-residue-soil system I. Theory and development. Trans. ASAE 32 (2), 565–0571. https://doi.org/10.13031/2013.31040.

Gao, H., et al., 2022. Frozen soil hydrological modeling for a mountainous catchment northeast of the Qinghai–Tibet Plateau. Hydrol. Earth Syst. Sci. 26 (15), 4187–4208. https://doi.org/10.5194/hess-26-4187-2022.

Gao, H., et al., 2023. Impacts of seasonally frozen soil hydrothermal dynamics on the watershed hydrological processes inferred from a spatially distributed numerical modelling approach. J. Hydrol. 624, 129947. https://doi.org/10.1016/j.jhydrol.2023.129947.

Gao, Z., Lin, Z., Niu, F., Luo, J., 2020. Soil water dynamics in the active layers under different land-cover types in the permafrost regions of the Qinghai–Tibet Plateau, China. Geoderma 364, 114176. https://doi.org/10.1016/j.geoderma.2020.114176.

Hansson, K., Imnek, J., Mizoguchi, M., Lundin, L.C., Genuchten, M.T., 2004. Water flow and heat transport in frozen soil: numerical solution and freeze-thaw applications. Vadose Zone J. 3 (2), 693–704.

Hu, G., et al., 2015. Modeling permafrost properties in the Qinghai-Xizang (Tibet) Plateau. Sci. China Earth Sci. 58 (12), 2309–2326. https://doi.org/10.1007/s11430-015-5197-0.

Hu, G., et al., 2023. Water and heat coupling processes and its simulation in frozen soils: current status and future research directions. CATENA 222, 106844. https://doi.org/10.1016/j.catena.2022.106844.

Iwata, Y., Hayashi, M., Hirota, T., 2008. Effects of snow cover on soil heat flux and freeze-thaw processes. J. Agric. Meteor. 64, 301–309.

Jansson, P.E., 2012. CoupModel: model use, calibration, and validation. Trans. ASABE 55 (4), 1335–1344.

Lamontagne-Hallé, P., McKenzie, J.M., Kurylyk, B.L., Zipper, S.C., 2018. Changing groundwater discharge dynamics in permafrost regions. Environ. Res. Lett. 13 (8), 084017. https://doi.org/10.1088/1748-9326/aad404.

Langford, J.E., Schincariol, R.A., Nagare, R.M., Quinton, W.L., Mohammed, A.A., 2020. Transient and transition factors in modeling permafrost thaw and groundwater flow. Groundwater 58 (2), 258–268. https://doi.org/10.1111/gwat.12903.

Li, X., Jin, R., Pan, X., Zhang, T., Guo, J., 2012. Changes in the near-surface soil freeze–thaw cycle on the Qinghai-Tibetan Plateau. Int. J. Appl. Earth Obs. Geoinf. 17, 33–42. https://doi.org/10.1016/j.jag.2011.12.002.

Lu, T., et al., 2025. Divergent effect of the freeze–thaw process on soil moisture dynamics in an alpine region of the northeast Qinghai-Tibet plateau. CATENA 258, 109288. https://doi.org/10.1016/j.catena.2025.109288.

Ming, J., Zhao, Y., Wu, Q., He, H., Gao, L., 2022. Soil temperature dynamics and freezing processes for biocrustal soils in frozen soil regions on the Qinghai–Tibet Plateau. Geoderma 409, 115655. https://doi.org/10.1016/j.geoderma.2021.115655.

Nash, J.E., Sutcliffe, J.V., 1970. River flow forecasting through conceptual models part I — A discussion of principles. J. Hydrol. 10 (3), 282–290. https://doi.org/10.1016/0022-1694(70)90255-6.

Peng, X., et al., 2016. Response of changes in seasonal soil freeze/thaw state to climate change from 1950 to 2010 across china. J. Geophys. Res. Earth Surf. 121 (11), 1984–2000. https://doi.org/10.1002/2016jf003876.

Peng, X., et al., 2017. Response of seasonal soil freeze depth to climate change across China. Cryosphere 11 (3), 1059–1073. https://doi.org/10.5194/tc-11-1059-2017.

Rooney, E.C., et al., 2022. Soil pore network response to freeze-thaw cycles in permafrost aggregates. Geoderma 411, 115674. https://doi.org/10.1016/j.geoderma.2021.115674.

Shur, Y.L., Jorgenson, M.T., 2007. Patterns of permafrost formation and degradation in relation to climate and ecosystems. Permafr. Periglac. Process. 18 (1), 7–19. https://doi.org/10.1002/ppp.582.

Sun, L., et al., 2021. Effect of freeze-thaw processes on soil water transport of farmland in a semi-arid area. Agric. Water Manag. 252. https://doi.org/10.1016/j.agwat.2021.106876.

Tian, J., Zhang, B., He, C., Yang, L., 2017. Variability in soil hydraulic conductivity and soil hydrological response under different land covers in the Mountainous Area of the Heihe River Watershed, Northwest China. Land Degrad. Dev. 28 (4), 1437–1449. https://doi.org/10.1002/ldr.2665.

Walvoord, M.A., Kurylyk, B.L., 2016. Hydrologic impacts of thawing permafrost—a review. Vadose Zone J. 15 (6), vzj2016.01.0010. https://doi.org/10.2136/vzj2016.01.0010.

Wang, G., et al., 2023b. Study on water and heat transport of different types of vegetations and fields in Pengbo alpine irrigation district of Qinghai Tibet Plateau. J. Hydrol. 618, 129201. https://doi.org/10.1016/j.jhydrol.2023.129201.

Wang, G., et al., 2023a. Responses of freeze-thaw process and hydrothermal variations within soil profiles to the cultivation of forest and grassland in Northeast China. Soil Tillage Res. 228. https://doi.org/10.1016/j.still.2023.105653.

Wang, G., Mao, T., Chang, J., Song, C., Huang, K., 2017. Processes of runoff generation operating during the spring and autumn seasons in a permafrost catchment on semi-arid plateaus. J. Hydrol. 550, 307–317. https://doi.org/10.1016/j.jhydrol.2017.05.020.

Wang, K., Zhang, T., Zhong, X., 2015. Changes in the timing and duration of the near-surface soil freeze/thaw status from 1956 to 2006 across China. Cryosphere 9 (3), 1321–1331. https://doi.org/10.5194/tc-9-1321-2015.

Wang, T., et al., 2019a. The effects of freeze-thaw process on soil water migration in dam and slope farmland on the Loess Plateau, China. Sci. Total Environ. 666, 721–730. https://doi.org/10.1016/j.scitotenv.2019.02.284.

Wang, X., et al., 2019b. Changes in river discharge in typical mountain permafrost catchments, northwestern China. Quat. Int. 519, 32–41. https://doi.org/10.1016/j.quaint.2018.11.010.

Wang, X., Gao, B., 2022. Frozen soil change and its impact on hydrological processes in the Qinghai Lake Basin, the Qinghai-Tibetan Plateau, China. J. Hydrol. Reg. Stud. 39, 100993. https://doi.org/10.1016/j.ejrh.2022.100993.

Wang, X., Wang, C., Wang, X., Huo, Z., 2020. Response of soil compaction to the seasonal freezing-thawing process and the key controlling factors. CATENA 184, 104247. https://doi.org/10.1016/j.catena.2019.104247.

Wu, T., Li, H., Lyu, H., 2023. Effect of freeze–thaw process on heat transfer and water migration between soil water and groundwater. J. Hydrol. 617, 128987. https://doi.org/10.1016/j.jhydrol.2022.128987.

Yang, L., et al., 2017. Identifying separate impacts of climate and land use/cover change on hydrological processes in upper stream of Heihe River, northwest China. Hydrol. Process 31, 1100–1112. https://doi.org/10.1002/hyp.11098.

Yang, L., et al., 2020. Regional hydrology heterogeneity and the response to climate and land surface changes in arid alpine basin, northwest China. CATENA 187, 104345. https://doi.org/10.1016/j.catena.2019.104345.

Yang, L., et al., 2024. Attributing the streamflow variation by incorporating glacier mass balance and frozen ground into the Budyko framework in alpine rivers. J. Hydrol. 628, 130438. https://doi.org/10.1016/j.jhydrol.2023.130438.

You, Q., Xue, X., Peng, F., Dong, S., Gao, Y., 2017. Surface water and heat exchange comparison between alpine meadow and bare land in a permafrost region of the Tibetan Plateau. Agric. For. Meteor. 232, 48–65. https://doi.org/10.1016/j.agrformet.2016.08.004.

Zhao, L., et al., 2024. Investigation, monitoring, and simulation of permafrost on the Qinghai-Tibet plateau: a review (n/a(n/a)). Permafr. Periglac. Process.. https://doi.org/10.1002/ppp.2227.

Zhao, Y., Nan, Z., Ji, H., Zhao, L., 2022. Convective heat transfer of spring meltwater accelerates active layer phase change in Tibet permafrost areas. Cryosphere 16 (3), 825–849. https://doi.org/10.5194/tc-16-825-2022.

Zheng, C., et al., 2023. Water transfer mechanisms and vapor flow effects in seasonally frozen soils. J. Hydrol. 627, 130401. https://doi.org/10.1016/j.jhydrol.2023.130401.

Zou, D., et al., 2017. A new map of permafrost distribution on the Tibetan Plateau. Cryosphere 11 (6), 2527–2542. https://doi.org/10.5194/tc-11-2527-2017.